國立清華大學

物理系

碩士學位論文

個體差異性對交通系統內相變的影響

Effect of individual difference on the jamming transition in traffic flow

學號姓名：108022503 賴易杰 (Yi-Chieh Lai)

指導教授：吳國安 (Kuo-An Wu)

中 華 民 國 一 一〇 年 六 月

Effect of individual difference on the jamming transition in traffic flow

A Thesis Presented to

the Department of Physics at

National Tsing Hua University

in Partial Fulfillment for the Requirement of

the Master of Science Degree Program

By

Yi-Chieh Lai

Advisor

Prof. Kuo-An Wu

June 2021

Abstract

The individual difference, particularly in drivers' distance perception, is introduced in the microscopic one-dimensional optimal velocity model to investigate its effect on the onset of the jamming instability seen in traffic systems. We show analytically and numerically that the individual difference helps to inhibit the traffic jam at high vehicle densities while it promotes jamming transition at low vehicle densities. In addition, the jamming mechanism is further investigated by tracking how the spatial disturbance travels through traffics. We find that the jamming instability is uniquely determined by the overall distribution of drivers' distance perception rather than the spatial ordering of vehicles. Finally, a generalized form of the optimal velocity function is considered to show the universality of the effect of the individual difference.

Keywords. active matter, traffic model, phase transition, individual difference

摘要

藉由將個體差異性引入一維微觀尺度的交通模型，我們同時定性與定量上分析個體差異性如何影響交通系統。我們發現在高密度的情況下存在適當個體差異性可以有效降低交通系統的不穩定度，並減緩塞車的現象。此外，我們藉由研究高密度車流如何在交通系統中傳播發現一個系統的發生塞車與否只和個體差異如何被選取有關，與個體差異如何在空間中分佈並無太大關連。最後，此理論所推導出的結果可以被拓展至其他具有同性質的交通模型上。

Acknowledgements

非常感謝我的指導教授-吳國安教授，在我碩士研究生涯中給予我許多寶貴的指導與意見。從一開始，教導我研究領域上的基礎知識與與研究方法，還有之後進行研究的數值模擬與理論分析，使我獲益良多。同時，也也感謝同研究團隊裡的劉明威學長、吳尚融學長、柯冠宇學長、劉沛弦同學和王治鈞學弟在研究上的幫助，在討論中給予我珍貴的意見與想法。最後，感謝我的家人在這段時間以來給我的支持與鼓勵。

Contents

List of Tables

List of Figures

Notation

Table 1: Notation Table. This table only includes parameters that are crucial to this article. The definition of few parameters, which are not included in this table, can be found in the chapter that these parameters first appear.

Symbol	The physical meaning of the parameter
L	The length of the track.
N	The number of vehicles in the system.
τ	Drivers' reaction time.
Δx_n	The interval between the n^{th} driver and the $(n+1)^{th}$ driver.
v_n	The velocity of the n^{th} driver.
Δv_n	The velocity difference between the n^{th} driver, and the $(n+1)^{th}$ driver. i.e. $\Delta v_n = v_{n+1} - v_n$
V	The desired velocity function.
$x_n^{(0)}$	The equilibrium position of the n^{th} driver.
y_n	The perturbation exerts on the n^{th} driver.
$\tilde{y}_k$	The k^{th} Fourier component of the perturbation.
w_n	The distance perception of the n^{th} driver.
$\tilde{w}_k$	The k^{th} Fourier component of the distance perception.
f_0	The derivative of desired velocity at equilibrium state divide by w, which is a constant when drives are identical. i.e. $\frac{1}{w}\frac{dV(w\Delta x)}{d\Delta x_n}\Big\vert_{\Delta x_n=\Delta x_n^{(0)}}$
f_1	The derivative of desired velocity at equilibrium state divide by w_n when the individual difference is taken into account. i.e. $\frac{1}{w_n}\frac{dV(w_n\Delta x_n)}{d\Delta x_n}\Big\vert_{\Delta x_n=\Delta x_n^{(0)}}$
$\bar{w}$	The mean value of the distance perception.

σ	The standard deviation of the distance perception.

Chapter 1

Introduction

In recent years, researches on the active system have attracted tons of interest due to several reasons, such as the existence of multiple degrees of freedom and self-driven properties. One of the most fascinating features of this system is that they typically exhibit a spontaneous phase transition from a uniform state into an inhomogeneous state [3, 4].

The traffic system is one of the most well-studied active systems, of which the studies dates back to the early 20th century. It perfectly illustrates the dynamical transition to a jammed state even before the road capacity is reached, as everyone experiences on a daily basis [5, 6]. The jamming transition could be attributed to various factors such as car accidents, traffic bottlenecks, etc. Besides that, sometimes, the traffic jam could also occur for no apparent reasons, which is known as the "phantom traffic jam".

An understanding of the underlying dynamics can begin with mathematical models that use different methodologies, such as microscopic particle-based models [7, 8, 9, 10, 11, 12, 13, 14, 15] which model vehicles in a traffic system as interacting particles. This method provides a way to investigate the detail mechanism behind jamming formation. However, this method faces difficulties in terms of simulation when the number of vehicles increases. Another perspective that approximates the traffic system with an acceptable amount of information loss is the macroscopic continuum models [16, 17, 18], in which traffic systems are described as a hydrodynamic-like system. With the help of continuity equations and Navier-Stokes like equations, one can specify the state of a traffic system.

Obviously, the deficiency of the macroscopic models is that the details regarding the mechanism behind jamming transition is obscured. To overcome this problem, other models such as mesoscopic Boltzmann-like models [19, 20] were developed. Even though this method provides a way to fomulate the relationship between the driver's behavior and jamming formation in the thermodynamic limit, it still has no choice but to use certain artificial assumptions, such as assuming Gaussian-like velocity distributions in order to specify traffic states. Since the investigation of the relationship between individual differences and jamming formations is what we desire, due to the reasons mentioned above, the choice of the microscopic model can help us to understand the mechanism behind it.

One of the successful microscopic models, is the so called optimal velocity model proposed by Bando *et al.* [11], where a headway-dependent optimal velocity is put into the equation of motion and the individual difference of drivers is discarded for simplicity. Bando *et al.* showed analytically and numerically that traffic congestion is spontaneously induced when the relaxation time of drivers is slower than the rate of change in the optimal velocity as the distance to the vehicle in the front changes. In addition, Bando *et al.* showed that the inhomogeneous state formed in the model is composed of two different states: a free flow state and a congested state with two specific propagation velocities, which is consistent with the observation of highway traffic [21, 22, 23]. Besides the headway-dependent optimal velocity, there are other realistic factors being considered in traffic models, such as the relative-velocity dependent optimal velocity [14], the lane-changing effect in a multi-lane traffic system [24, 25], the size effect due to multi-species vehicles [26, 27, 28], temperament of drivers [29, 30], etc.

Regardless, the assumption of identical drivers is commonly employed in traffic models for simplicity. However, drivers are expected to perceive the change of surroundings differently as one would expect for different individual biological beings in general. Furthermore, it is shown that a wide scattering of synchronized states seen in the fundamental diagram can be reproduced for a traffic model considering a mixture of different vehicle types like cars and trucks, which indicates the importance of the individual difference [28]. Recent study by Tang *et al.* incorporated the individual difference of drivers' perception ability in the macroscopic contin-

uum model, which showcased the close relationship between individual differences and the scattered data in the fundamental diagram [31].

In this study, we investigate the effect of individual differences, in particular the drivers' distance perception, on jamming transition using Bando's microscopic model. We show analytically and numerically that the individual difference affects the phase transition significantly, and the individual difference always suppresses traffic jams at high vehicle densities. Furthermore, quiet interestingly, we found that the spatial ordering of drivers is irrelevant to the jamming transition.

This thesis is organized as follows: In Chapter 2, we briefly review the concepts of microscopic models and focus on the optimal velocity model by Bando *et al.*. In Chapter. 3, the individual difference in the drivers' distance perception is introduced using Gaussian random fields, and linear stability analysis combined with a perturbation theory are employed to investigate the effect of individual differences on the jamming transition quantitatively. To further understand the jamming mechanism, we take a closer look at how a headway disturbance travels through traffic. We find that the jamming transition is closely related to the overall distribution of drivers' distance perception rather than the spatial ordering of vehicles. Finally, we extend the optimal velocity model to show the universality of the effect of the individual difference in Sec. 3.2. The comparison between widely scattered empirical data and simulation results will be discussed in Chapter 4. In Chapter. 5, the summary and the discussion of each chapter will be included. Future works will also be suggested in this chapter.

Chapter 2

Bando's Model

In microscopic model, drivers in a traffic system are imagined as interacting particles. Each driver tries to adjust velocity according to the stimulus coming from the distance in front Δx, the relative velocity with leading vehicles Δv, and driver's velocity v. However, since there is reaction time preventing drivers adjust to the velocity they desired instantaneously, they will try to adjust their velocity to the desired velocity $V(\Delta x, \Delta v, v)$ coming from the condition τ times before, which means

$$v(t+\tau) = V(\Delta x, \Delta v, v), \tag{2.1}$$

where $V(\Delta x, \Delta v, v)$ is the desired velocity for driver in the condition $(\Delta x, \Delta v, v)$. If the reaction time is small enough, equation (2.1) can be expanded as

$$\frac{dv}{dt} = \frac{V(\Delta x, \Delta v, v) - v}{\tau}, \tag{2.2}$$

which represents the driver will relax to the desired velocity in the time scale τ. To prevent confusion, in the remaining article, τ in Eq. (2.2) like equations will be called "relaxation time" to compare with "reaction time" in Eq. (2.1) like equations. Though there are many choices about desired velocity; however, they should at least satisfy the following rules. First of all, to avoid accidents, the desired velocity should tend to zero when the distance in front decrease to zero, which means $\lim_{\Delta x \to 0} V(\Delta x, \Delta v, v) = 0$. Secondly, even though there is no vehicles in front, the driver will never infinitely accelerate. Therefore, $\lim_{\Delta x \to \infty} V(\Delta x, \Delta v, v) = V_{\max}$ where $V_{\max}$ is the maximum velocity due to speed regulation, car performance, and so forth.

In 1995, Bando *et al.* proposed a well-known optimal velocity model with N vehicles in a surpassing prohibited, single lane closed loop of length L, in which and the driver of $n-th$ vehicle adjusts its velocity v_n only according to its distance to the vehicle in front, $\Delta x_n = x_{n+1} - x_n$, where x_n is the location of $n-th$ vehicle[11]. Therefore,

$$\ddot{x}_n = \frac{V\left(w\Delta x_n\right) - \dot{x}_n}{\tau}. \tag{2.3}$$

A simple optimal velocity function introduced by Bando *et al.* is

$$V\left(\Delta x_n\right) = \tanh\left(w\Delta x_n - h\right) + \tanh\left(h\right).$$

It is clear that the choice of desire velocity satisfies the two necessary rules. Two parameters, w and h, are chosen to describe the behavior of drivers. The shift of hyperbolic tangent h describes the condition when there is small interval in front, drivers tend to maintain small velocity until a comfortable distance is reached. The other parameter, w, describes the distance perception of driver. Obviously, drivers with large w (poor distance perception) adjust their velocity more abruptly than those with small w (well distance perception) when the distance in front decreases by the same amount; and w is always positive. The dynamical behavior of this system is readily obtained by linear stability analysis around homogeneous state. For identical drivers, the homogeneous state is drivers with equal distance and driving with same velocity, which means

$$x_n^{(0)}\left(t\right) = nb + V\left(b\right)t, \tag{2.4}$$

where $b = L/N$ represents equal distance in equilibrium state. Now assume small fluctuation is applied to the equilibrium state of this system, $x_n\left(t\right) = x_n^{(0)}\left(t\right) + y_n\left(t\right)$. Inserting fluctuations into equation (2.3), a linearized equation of y_n will be obtained as

$$\ddot{y}_n = \frac{1}{\tau} w f_0 \Delta y_n - \frac{1}{\tau}\dot{y}_n, \tag{2.5}$$

where

$$f_0 \equiv \frac{1}{w}\frac{dV(w\Delta x_n)}{d\Delta x_n}\bigg|_{\Delta x_n = \Delta x_n^{(0)}}. \tag{2.6}$$

Due to the closed loop boundary condition, N coupled equations (2.5) can be easily analyzed in the Fourier space,

$$y_n = \sum_{k=-N/2+1}^{N/2} \tilde{y}_k e^{i\alpha_k n}, \tag{2.7}$$

where $\alpha_k = 2\pi k/N$. In Fourier space, equation (2.5) can be rewritten as

$$\ddot{\tilde{y}}_k + \frac{1}{\tau}\dot{\tilde{y}}_k = \frac{wf_0}{\tau}\left(e^{i\alpha_k} - 1\right)\tilde{y}_k. \tag{2.8}$$

Apparently, equations in Fourier coordinates are decoupled with each others. It turns out to be an eigenvalue problem in which eigenvalue with largest real part onset the instability of this system, and solutions can be deduced by setting $\tilde{y}_k \propto e^{z_k t}$. Since the neutral stability condition occurs when the perturbation neither growth nor decay, which means the real part of z_k should be zero, we can suppose a pure imaginary eigenvalue $z_k = iu_k$ to deduce the neutral stability condition. The real part and imagine part of equation (2.8) becomes

$$\begin{cases} -u_k^2 = wf_0\left(\cos\alpha_k - 1\right)/\tau \\ u_k/\tau = \frac{f_0}{\tau}\sin\alpha_k \end{cases}. \tag{2.9}$$

Eliminating the variable u_k, the neutral stability condition can be obtained, and the instability will occur when

$$f_0 > \frac{1}{2\tau\cos^2\left(\alpha_k/2\right)} \tag{2.10}$$

is satisfied. The physical interpretation of instability condition can be realized as the competition between two time scales, τ and $1/f_0$. The first time scale τ represents the relaxation time of drivers. The second time scale $1/f_0$ describes how abrupt drivers change their desired velocity when the distance in front changes. As the relaxation time τ becomes larger than $1/f_0$, drivers can't adjust their velocities fast enough as they desired, then instability occurs. The simulation results that are reproduced by us can be seen in Fig. 2.1 and 2.2.

Evidently, the choices of desired velocity influences the evolution of the traffic system and are usually set to fit the phenomenological experiments data[14, 32]. However, the instability can be always realized as the competition between the relaxation times and others time scales whatever the model is chosen.

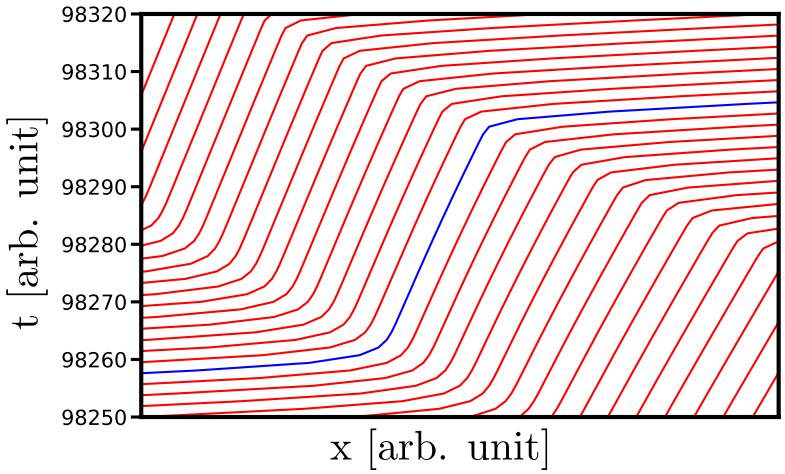

Figure 2.1: Simulation results of jamming transition in the system with global density set to 1 and total vehicles number set to 32. This figure only shows part of the simulation results, and mainly focus on one duration in which the jamming transition has occurred. Each line presents the trajectory of a single vehicle. The blue line is the trajectory of the 15^{th} vehicle. The velocity of this vehicle dramatically decreases in the period of $98260 < t < 98300$. The inverse of reaction time is set to be 0.01 lower than the threshold of the neutral stability condition.

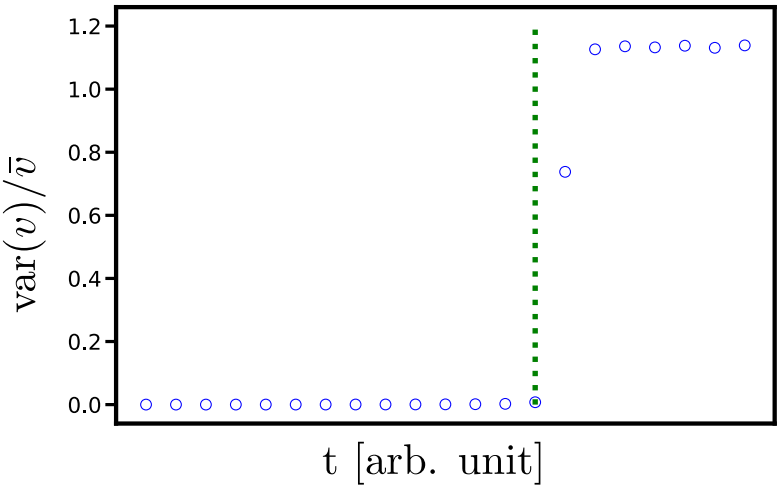

Figure 2.2: Simulation results show that jamming transition occurs with increasing velocity variance. Jamming state in a closed loop is composed of two states: the free flow and jamming cluster states, which means that the variance of velocity is different between the unjammed state and jammed state. Blue circles show how velocity variance varies with time in a system with the same configuration as Fig 2.1. The Green dashed line shows the onset of jamming transition.

Tough Bando's model is mathematically simple, it is usually criticized for poor descriptions of real data. For instance, since the vehicle number is conserved in Bnado's model, it is hardly possible to reproduce the so-called "synchronized flow", which shows the growing jamming region whose wave front is usually stationary on the traffic bottleneck, such as ramps or shrinking of highway [33]. Other realistic factors, such as open boundary conditions [34], also show insufficiences of Bando's model. Nonetheless, Bondo's model still provides a possible way to understand how these realistic factors influence the onset of instability. Since our research topic is investigating how heterogeneity of traffic system due to individual difference affects the onset of instability, some modifications of Bando's are done in our researches.

In the next section, the consideration of different driving behavior in a single system will be considered, which means there are multiple time scales in a system should be considered. The analytical and numerical results show the possibility of jamming suppression due to the existence of such individual difference effect.

Chapter 3

Effect of Individual Difference

3.1 Individual Difference

In the original optimal velocity model, one assumes that all drivers obey the same acceleration rules. However, in reality, drivers exhibit different levels of distance perception, hence different degrees of abruptness for drivers to adjust the velocity are expected. In this section, we introduce individual difference, specifically the difference in distance perception, to the optimal velocity model. We show that individual difference in distance perception helps to prevent traffic jam in the heavy traffic regime as discussed in detail below.

3.1.1 Linear Stability Analysis

The individual difference is introduced into the optimal velocity model by assigning different value of w to each driver. Therefore, Eq. (2.3) becomes

$$\ddot{x}_n = \frac{V(w_n \Delta x_n) - \dot{x}_n}{\tau}, \tag{3.1}$$

where

$$V(w_n \Delta x_n) = \tanh(w_n \Delta x_n - h) + \tanh(h). \tag{3.2}$$

It is apparent that even if Δx_n's are the same, drivers would have different desired velocity $V(w_n \Delta x_n)$ due to different distance perception. Although drivers are different from one another, it does not seem too far-fetched to assume a simple Gaussian distribution for w_n. For simplicity, we assume a Gaussian distribution for w_n with mean $\bar{w} = 1$ and standard deviation σ. The steady state of the system

is obtained by requesting $\ddot{x}_n = 0$ in Eq. (3.1). That is all drivers moving with the same velocity but different distance to the vehicle in front, which means

$$w_n \Delta x_n^{(0)} = \text{Constant} \tag{3.3}$$

With the constraint of the total length of closed loop $\sum_n \Delta x_n = L$, we obtain

$$x_n^{(0)} = \sum_{i=1}^{n} \Delta x_i^{(0)} + v^{(0)} t, \tag{3.4}$$

where we set the location of the first vehicle to be at the origin of the moving frame, and

$$\Delta x_i^{(0)} = \frac{L}{w_i} \left(\sum_j \frac{1}{w_j} \right)^{-1}, \tag{3.5}$$

$$v^{(0)} = V(w_n \Delta x_n^{(0)}). \tag{3.6}$$

Similarly, we assume a perturbation $y_n(t)$ around the steady state, hence the location of the nth vehicle is $x_n(t) = x_n^{(0)} + y_n(t)$. Then the linearized equation of $y_n(t)$ is readily obtained

$$\ddot{y}_n + \frac{1}{\tau}\dot{y}_n = \frac{f_1}{\tau} w_n \Delta y_n, \tag{3.7}$$

where

$$f_1 = \frac{1}{w_n} \frac{\partial V(w_n \Delta x_n)}{\partial \Delta x_n}\bigg|_{\Delta x_n = \Delta x_n^{(0)}} = \operatorname{sech}^2(w_n \Delta x_n^{(0)} - h). \tag{3.8}$$

Substitute the Fourier expansion of $y_n(t)$, Eq. (2.7), into Eq. (3.7), we obtain

$$\ddot{\tilde{y}}_k + \frac{1}{\tau}\dot{\tilde{y}}_k = \frac{f_1}{\tau} \sum_\ell \tilde{y}_\ell \tilde{w}_{k-\ell} \big(\exp(i\alpha_\ell) - 1 \big), \tag{3.9}$$

where $\tilde{w}_m$ is the mth Fourier amplitude of the Fourier transform of w_n's,

$$w_n = \sum_{m=-N/2+1}^{N/2} \tilde{w}_m e^{i\alpha_m n}. \tag{3.10}$$

It is interesting to note that Eq. (3.9) shows an intricate coupling between the dynamics of perturbations and the spatial distribution of different distance perception of drivers. It becomes an eigenvalue problem of coupled equations with N degrees of freedom. And the eigenvalues clearly depend on how w_n's are distributed. To generate spatially random and uncorrelated w_n's, we employ the Gaussian random field with mean $\bar{w}$ and standard deviation σ. The Gaussian

random field is much easier to be produced in the Fourier space, see Ref. [35]; the ensemble average of the squared magnitude of the Fourier amplitude of the individual difference $\tilde{w}_k$ is associated with $\bar{w}$ and σ.

The calculation can be separated into two conditions:

Let's define

$$M \equiv \int \prod_i \exp\left(-\frac{(w_i-\bar{w})^2}{2\sigma^2}\right) dw_i$$

(1) $k=0$

$$\begin{aligned}\langle|\tilde{w}_{k=0}|^2\rangle &= \int \tilde{w}_0\tilde{w}_0^* \prod_i \exp\left(-\frac{(w_i-\bar{w})^2}{2\sigma^2}\right) dw_i \Big/ M \\ &= \bar{w}^2. \end{aligned} \tag{3.11}$$

(2) $k\neq 0$

$$\begin{aligned}\langle|\tilde{w}_{k\neq 0}|^2\rangle &= \int \tilde{w}_k\tilde{w}_k^* \prod_i \exp\left(-\frac{(w_i-\bar{w})^2}{2\sigma^2}\right) dw_i \Big/ M \\ &= \frac{1}{N^2}\sum_n\sum_m e^{i\alpha_k(n-m)} \int w_n w_m \prod_i \exp\left(-\frac{(w_i-\bar{w})^2}{2\sigma^2}\right) dw_i \Big/ M \\ &= \frac{1}{N^2}\left[\bar{w}^2\sum_{n\neq m} e^{i\alpha_k(n-m)} + \left(\bar{w}^2+\sigma^2\right)\sum_{n=m} e^{i\alpha_k(n-m)}\right] \\ &= \frac{\bar{w}^2}{N^2}\sum_{n,m} e^{i\alpha_k(n-m)} + \frac{\sigma^2}{N} \\ &= \frac{\sigma^2}{N}. \end{aligned} \tag{3.12}$$

It shows that the Fourier amplitude of the non-zero wavenumber mode would be much smaller than that of zero wavenumber mode as N gets larger. Therefore, we can analyze the system perturbatively by separating the coupling terms into the unperturbed part which only associated with $\tilde{w}_0$ (note that $\tilde{w}_0=\bar{w}$) and the perturbed part which associated with $\tilde{w}_{k\neq 0}$. By defining $\tilde{\mathbf{y}}^T = (\tilde{y}_{-N/2+1}, \tilde{y}_{-N/2+2}, \cdots, \tilde{y}_{N/2})$, Eq. (3.9) can be re-written as

$$\frac{d^2}{dt^2}\tilde{\mathbf{y}} + \frac{1}{\tau}\frac{d}{dt}\tilde{\mathbf{y}} = \frac{f_1}{\tau}(H^0+H^1)\tilde{\mathbf{y}}, \tag{3.13}$$

where

$$H^0_{k\ell} = \tilde{w}_0\big(\exp(i\alpha_\ell)-1\big)\delta_{k\ell}, \qquad H^1_{k\ell} = \tilde{w}_{k-\ell}\big(\exp(i\alpha_\ell)-1\big)(1-\delta_{k\ell}). \tag{3.14}$$

Obviously, H^0 is treated as the unperturbed diagonal matrix, while H^1 is treated as the perturbed off-diagonal matrix. The eigenvalues of the unperturbed matrix are exactly the eigenvalues for the original optimal velocity model where the individual difference is absent. Note that, for each realization of the Gaussian random field, $f_1 = \mathrm{sech}^2(w_n \Delta x_n^{(0)} - h)$ would be slightly different due to the finite size effect. However, if the variance of the Gaussian distribution is small, we can approximate Eq. (3.5) as

$$w_n \Delta x_n^{(0)} = L \left(\sum_j \frac{1}{w_j} \right)^{-1} \approx \frac{L\tilde{w}_0}{N(1 + (\sigma/\tilde{w}_0)^2)}, \tag{3.15}$$

which always leads to a smaller value compared to the case of identical drivers ($\sigma = 0$). Therefore, a different value of f_1 is expected, and the neutral stability boundary of the system would differ from that for identical drivers.

Next, we proceed to discuss the correction to eigenvalues due to H^1. The stability analysis for the original optimal velocity model shows that the most unstable Fourier mode occurs for the longest finite wavelength mode, see Eq. (2.10). Since the perturbation does not affect the system dramatically, the stability of the system can be determined once the correction to the eigenvalue for the longest finite wavelength mode is known. The first order correction vanishes, since $\langle \phi_1 | H^1 | \phi_1 \rangle = 0$ due to the fact that H^1 is an off-diagonal matrix and $|\phi_1\rangle$ is an eigenvector composed solely of $\tilde{y}_1$. The second order correction to the eigenvalue is $\lambda_1^{(2)}$,

$$\lambda_1^{(2)} = \sum_{k \neq 1} \frac{|\tilde{w}_{1-k}|^2 (e^{i\alpha_k} - 1)(e^{i\alpha_1} - 1)}{\tilde{w}_0 (e^{i\alpha_1} - e^{i\alpha_k})} \simeq -\frac{i\sigma^2}{\tilde{w}_0} \sin \alpha_1. \tag{3.16}$$

See Appendix A. Hence, the governing equation of $\tilde{y}_1$, see Eq. (3.13), up to second order perturbation is

$$\ddot{\tilde{y}}_1 + \frac{1}{\tau} \dot{\tilde{y}}_1 \simeq \frac{f_1}{\tau} \tilde{w}_0 \left(\cos \alpha_1 - 1 + i \left(1 - \frac{\sigma^2}{\tilde{w}_0^2} \right) \sin \alpha_1 \right), \tag{3.17}$$

and the instability condition is modified accordingly,

$$f_1 > \frac{1}{2\tau \tilde{w}_0 (1 - \sigma^2/\tilde{w}_0^2)^2 \cos^2(\alpha_1/2)}. \tag{3.18}$$

Note that $w_n \Delta x_n^{(0)}$ also depends on $\sigma^2/\tilde{w}_0^2$, see Eq. (3.15), therefore it is expected that the neutral stability boundary varies as a function of $\sigma^2/\tilde{w}_0^2$ according to the above perturbation calculation. Fig. 3.1 shows how the phase boundary changes

with the individual difference. The threshold value of the reaction time τ of drivers increases as $\sigma/\tilde{w}_0$ increases for a specific vehicle density $N/L = 1$. At this vehicle density and for a non-vanishing value of $\sigma/\tilde{w}_0$, a higher threshold of reaction time of drivers is expected, which means the traffic system would remains unjammed even if the reaction of drivers becomes slower. In other words, the variation of distance perception of drivers helps to inhibit the onset of the traffic jam. As shown in Fig. 3.1, the area of the jammed state on the phase diagram reduces with $\sigma/\tilde{w}_0$, and the phase boundary is shown to vary quadratically with $\sigma/\tilde{w}_0$.

Evidently, there is deviation between the theoretical phase boundary and the simulation results when the individual difference increases. This comes from the fact that the technique we use to approach the analytical solution is perturbation method, and the strength of perturbation matrix is proportional to the square of individual difference σ^2. Therefore, as what we should expect, the analytical solution becomes invalid when the influence of individual difference becomes apparent. The suppression of jamming formations can be confirmed by inserting individual difference into a system, which is experiencing the jamming transition. See Fig. 3.2. This figure shows the fact that the existence of individual difference can effectively suppress the onset of instability. A quantitative analysis is shown in detail in the following section.

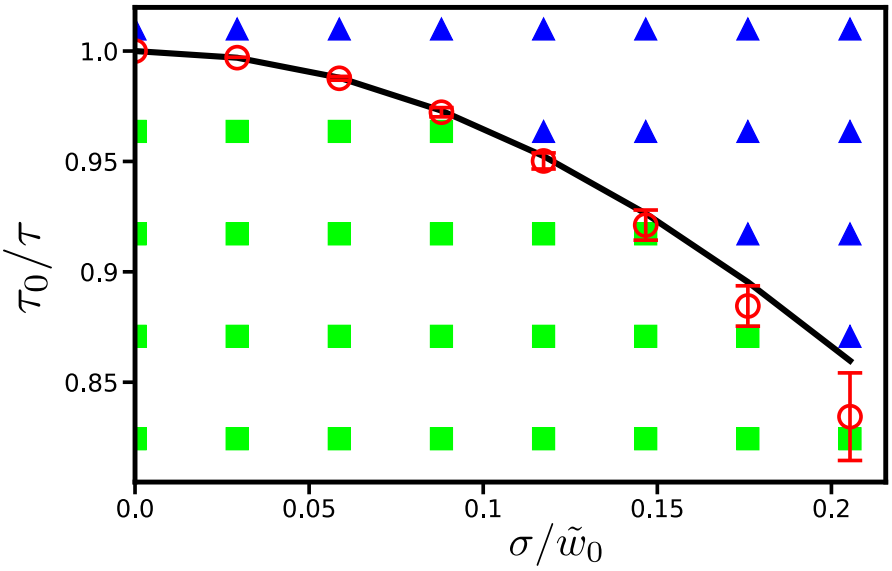

Figure 3.1: Phase diagram of the traffic system. Note that τ_0 is the threshold value of the reaction time when the individual difference is absent (i.e., $\sigma = 0$). The black line plots the neutral stability boundary of Eq. (3.18). Solid green squares and solid blue triangles represent the jammed and unjammed state, respectively, predicted from Eq. (3.18). Red circles are the simulation results of Eq. (3.1), which is consistent with the prediction obtained by solving the eigenvalue problem (not shown) of the coupled Eqs. (3.9). 100 realizations of Gaussian random fields are carried out for each simulation data point. The phase diagram is obtained for $N/L = 1$, $h = 2$, and $N = 512$.

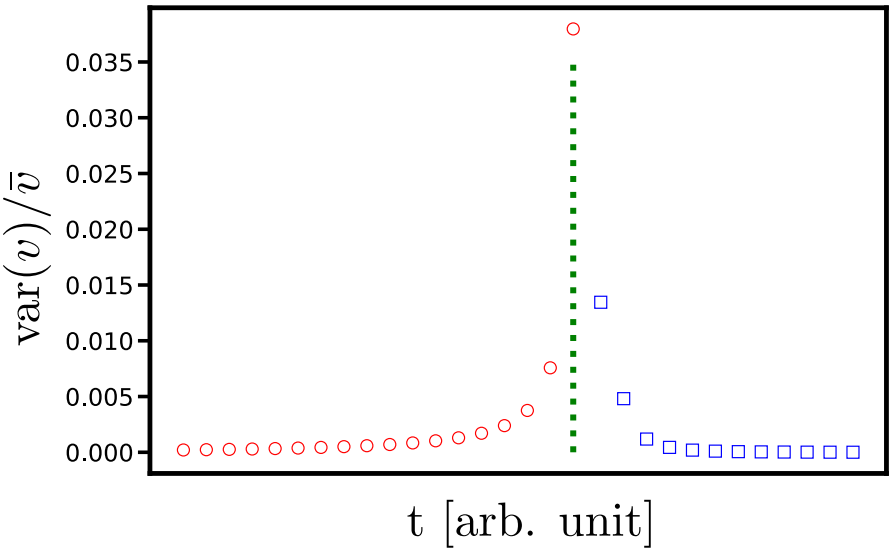

Figure 3.2: Jamming suppression due to the existence of individual difference. Red dots are simulation for identical drivers under the unstable condition $N = 32$, $L = 32$, and $a = 1$. After the variance of velocity increases over 0.035, the individual difference with $\sigma = 0.2$ is distributed to the system. Blue squares show the decreasing of velocity variance since individual difference is distributed to the system. Obviously, jamming transition is suppressed and the system returns to the free flow state.

The physical mechanism of the traffic jam can be analyzed by tracking how a spatial disturbance of the location of a vehicle, y_n, propagates through traffics. Since drivers adjust their speed according to the distance to the vehicle in front, the spatial disturbance of the location of one vehicle would give rise to a wave of disturbances travelling backward. Drivers with poor distance perception (larger w) tend to accelerate (or decelerate) more abruptly and overcorrect their speed. Therefore, the amplification of the spatial disturbance is expected if more poor distance perception drivers are in the traffic, which eventually leads to a traffic jam. On the other hand, the drivers with good distance perception (smaller w) would reduce the disturbance and keep the system stable. A quantitative analysis is given as follows.

3.1.2 Propagation of Disturbances

Now consider a system composed of N drivers with different w_n in a closed loop. All drivers are initially at their equilibrium locations, except the nth driver whose location is slightly off by the amount of y_n. Since all vehicles are in a closed loop, the spatial disturbance is expected to travel back to itself repeatedly. Therefore, one can assume $y_n = A_n(t)e^{i\Omega t} + c.c.$, where $A_n(t)$ is the amplitude of the disturbance wave and Ω characterizes the angular frequency of the wave, see Ref. [8].

Since we are looking for the stability of the system near the neutral stability boundary, A_n is expected to vary on a much slower time scale compared to $1/\Omega$. Therefore, by assuming a negligible time derivative of A_n on the time scale $1/\Omega$, we readily obtain, from Eq. (3.7), the disturbance propagation relation between A_{n-1} and A_n,

$$A_{n-1} = \frac{f_1 w_{n-1}}{R_{n-1}} e^{-i\theta_{n-1}} A_n, \tag{3.19}$$

where

$$R_{n-1} = \sqrt{(f_1 w_{n-1} - \Omega^2\tau)^2 + \Omega^2}, \tag{3.20}$$

$$\theta_{n-1} = \tan^{-1}\left(\frac{\Omega}{f_1 w_{n-1} - \Omega^2\tau}\right). \tag{3.21}$$

After the disturbance propagates through the traffic and come back to the nth vehicle, the amplitude A_n is amplified by a factor of $z \equiv \prod_{j=1}^{N}(f_1 w_j/R_j)$. Note that we have employed the fact that the sum of the phase difference θ_j over all vehicles is simply 2π. If z is greater than unity, the traffic jam occurs. Since the angular frequency of the wave decreases as the number of vehicles increase, in the thermodynamic limit, z can be well approximated by an expansion in terms of Ω^2 to the lowest order,

$$\begin{aligned} z &= \prod_n \frac{f_1 w_n}{\sqrt{\left(f_1 w_n - \Omega^2\tau\right)^2 + \Omega^2}} \\ &\simeq 1 - \frac{N}{2(f_1\tilde{w}_0)^2}\left[\left(1 + 3\frac{\sigma^2}{\tilde{w}_0^2}\right) - 2\tau(f_1\tilde{w}_0)\left(1 + \frac{\sigma^2}{\tilde{w}_0^2}\right)\right]\Omega^2. \end{aligned} \tag{3.22}$$

See Appendix 5. By requiring $z > 1$, it gives the criterion for the instability to occur

$$f_1 > \frac{1}{2\tau\tilde{w}_0}\left(1 + 2\frac{\sigma^2}{\tilde{w}_0^2}\right) + \mathcal{O}\left(\frac{\sigma^4}{\tilde{w}_0^4}\right), \tag{3.23}$$

which is consistent with Eq. (3.18) to the lowest order of $(\sigma/\tilde{w}_0)^2$ in the thermodynamic limit. To further explore the individual difference effect on the instability quantitatively, we expand f_1 in terms of $(\sigma/\tilde{w}_0)^2$. The neutral stability boundary is readily obtained to the lowest order of $(\sigma/\tilde{w}_0)^2$,

$$\frac{1}{\tau} = 2\,\mathrm{sech}^2(\gamma) + \beta\frac{\sigma^2}{{\tilde{w}_0}^2}, \tag{3.24}$$

where

$$\gamma = \frac{L\tilde{w}_0}{N},$$
$$\beta = 4\,\mathrm{sech}^2(\gamma - h)\Big(\gamma\tanh(\gamma - h) - 1\Big). \tag{3.25}$$

The inverse of the threshold value of the relaxation time τ is expected to exhibit a power law relation with $(\sigma/\tilde{w}_0)$. Simulation results for 512 vehicles of various densities are shown in Fig. 3.3; the inverse of the threshold value of τ is shown to be well fitted by a quadratic relation of $\sigma/\tilde{w}_0$ for $\log_{10}(\sigma/\tilde{w}_0) < -0.699$. It is interesting to note that the individual difference inhibits the onset of jamming instability at high vehicle densities where $\beta < 0$. Below a critical density where $\beta > 0$, the individual difference promotes the jamming transition instead.

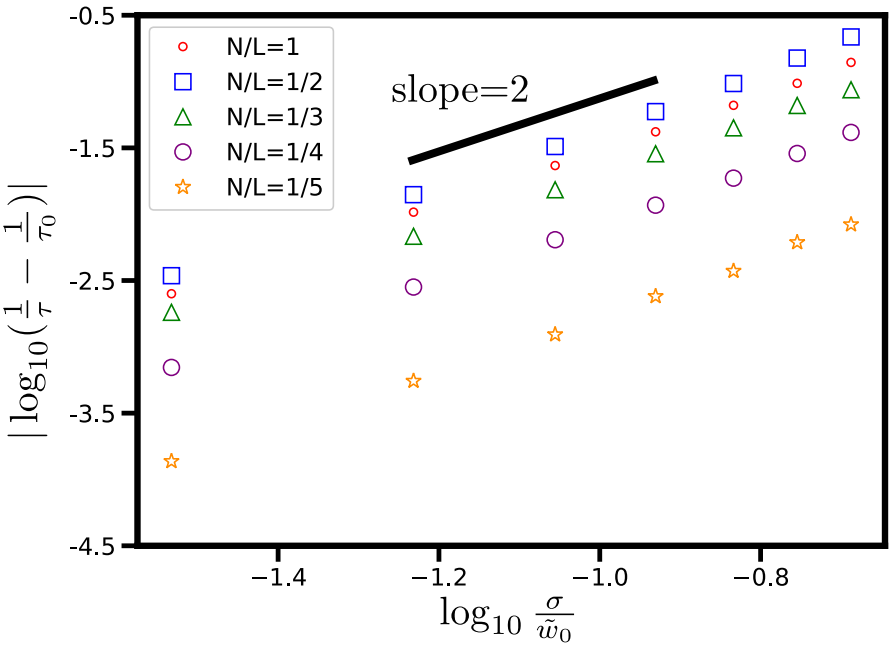

Figure 3.3: A log-log plot of simulation results of the deviation of $1/\tau$ from $1/\tau_0$ as a function of $\sigma/\tilde{w}_0$ for various global vehicle densities ranging from $N/L = 0.2$ to $N/L = 1$. The simulation results are well fitted by a power law relation with an exponent of 2. The simulation results are obtained with parameters $h = 2$ and $N = 512$.

Figure 3.4 shows how β changes with the inverse of the vehicle density. The value of β is always negative at high vehicle densities and positive at low vehicle densities regardless of the shift h of the velocity function, which can be understood as follows. The steady state velocity of vehicles for drivers with different distance perception is a bit smaller than that for identical drivers due to the decreasing distance to the front vehicle at equilibrium state compared with the distance when drives are identical, see Eq. (3.15). Since the onset of the instability comes down to the competition between the driver's reaction time and how fast the desired velocity changes as the distance to the front vehicle varies, a smaller interval means that drivers in the system will perceive density higher than the global density. This change will influence the system differently in the high and low densities. At high vehicle densities, the smaller interval will smoothen the desired velocity changes. However, at low vehicle densities, it will sharpen the changes. The underlying physics can be interpreted as follows: since drivers in a system with high density already drive slowly, they will drive even slower when they perceive

that the interval to the front vehicle decreases, and consequently smooth out the changes in their desired velocity. Therefore, the rate of change of the desired velocity is less sensitive to the distance change, which inhibits the traffic jam in high density regions. On the contrary, at low vehicle densities, since the decrease of the interval to the front vehicles causes drivers who can originally drive freely are thereby required to decelerate more drastically, which increases the changing rate of the desired velocity as the distance to the front varies. Thus, when compared to identical drivers, drivers with individual difference tend to decelerate or accelerate more abruptly as the distance to the front changes which makes the traffic system more vulnerable to the traffic jam.

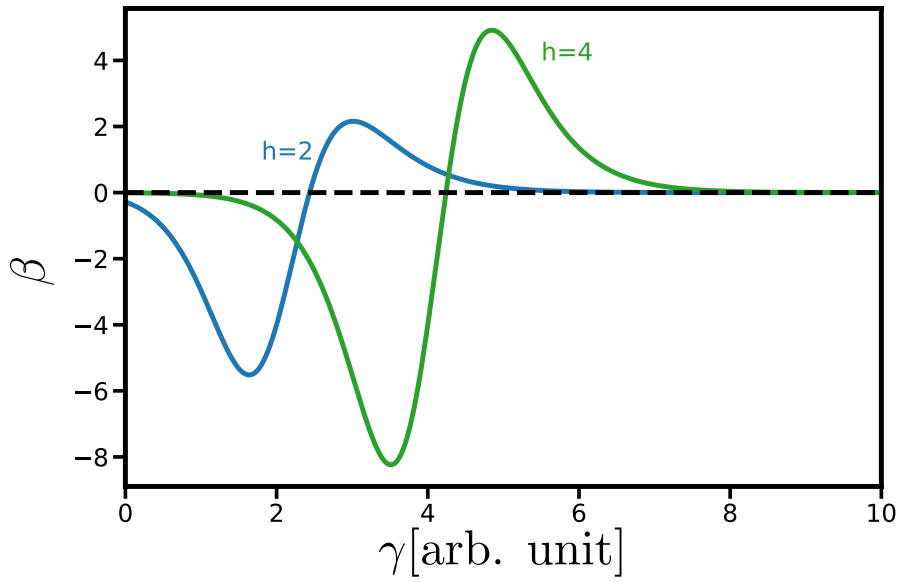

Figure 3.4: Plot of the coefficient β as a function of γ for different values of h. β is always negative at high vehicle densities which inhibits the jamming transition, while β becomes positive at low vehicle densities which promotes the jamming transition. The value of h characterizes the rate change of the velocity function as the headway changes which uniquely determines the critical vehicle density at which $\beta = 0$.

The Fig 3.4 also implies another important restriction to our analytical solutions. As what we mentioned in the previous section, the strength of second order perturbation is proportional to the square of individual difference. However, this figure shows that the coefficient of σ^2 will be zero under some conditions, which means the strength of second perturbation goes to zero, and our analytical predic-

tions will become invalid under these condition. To make the analytical solutions more accurate, one should take the next level of perturbation into consideration.

In this section, we propose another way to approach the neutral stability condition of jamming transition. The investigation of disturbance propagation not only help us to understand the mechanism behind jamming suppression due to the existence of individual difference but also simplify the calculation process. This method has significant advantage if we want to understand the mechanism of heterogeneity in models with complicated realistic factors. In order to discuss the universality of the effect of individual difference, in section 3.2, heterogeneity of different kinds of individual difference will be introduced, and the derivation of neutral stability condition is similar to the process in this section.

3.1.3 Irrelevance of Spatial Ordering of Vehicles

In the above analysis of disturbance propagation, the stability of a traffic system depends on the amplifying factor z, see Eq. (3.22), which involves a product of w_j/R_j of each vehicle. Since the product is invariant as one switches the spatial ordering of vehicles, the jamming transition of traffic systems is uniquely determined for the same group of drivers regardless of their spatial ordering. One could reach the same conclusion by solving the eigenvalue problem formulated before, see Eq. (3.7). For a given set of w_n's, the characteristic equation remains invariant as one reshuffles the spatial ordering of vehicles.

Figure 3.5 shows the simulation results of the amplitude for the slowest decaying eigenvector over time for 16 vehicles. The numerical simulations are carried out in the unjammed region that is close to the neutral stability boundary, and six different configurations of the spatial ordering of vehicles generated by random reshuffling are employed. In the linear regime, simulations show that dynamical behaviors for the slowest decaying eigenvector are identical for all six configurations. It is interesting to note that our calculation indicates that the stability of the traffic systems would be the same even for traffic systems that allow vehicles to switch order.

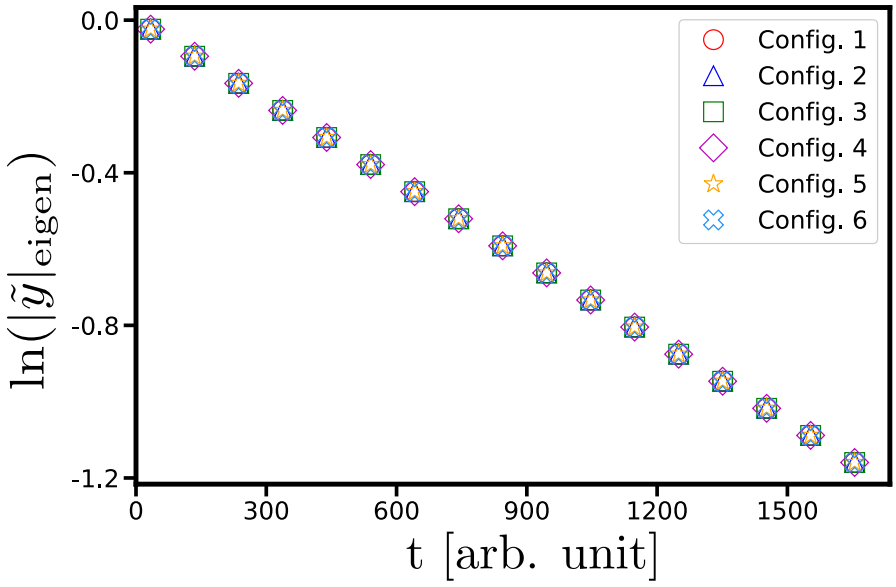

Figure 3.5: The amplitude of the slowest decaying eigenvector over time for simulations of 16 vehicles, $N/L = 1$, $\sigma/\tilde{w}_0 = 0.176$, and $\tau = 1.096$ in the unjammed region. Six different spatial configurations are generated by reshuffling the ordering of vehicles. Different symbols represent different configurations. Note that the amplitude oscillates with time, and only the peak values are shown.

3.2 Universality of The Effect of Individual Difference

It is intuitive that, in addition to the relative distance, the relative velocity to the vehicle in the front would also influence drivers' action to accelerate or decelerate. Based on the concept shown in Ref. [14, 32], we propose a generalized traffic model incorporated with the individual difference,

$$\ddot{x}_n = \frac{1}{\tau}\left[V_1(w_n\Delta x_n) + \lambda V_2(g_n\Delta v_n)e^{-w_n\Delta x_n/R} - \dot{x}_n\right], \tag{3.26}$$

where V_1 is the same optimal velocity function introduced before, $V_1(w_n\Delta x_n) = \tanh(w_n\Delta x_n - h) + \tanh(h)$. And the second term is the additional acceleration due to the relative velocity, where

$$V_2(g_n\Delta v_n) = \tanh(g_n\Delta v_n), \tag{3.27}$$

so that the driver slows down (speed up) when its velocity is faster (slower) than the vehicle in the front. Note that w_n's and g_n's are populated with Gaussian random fields with mean $\bar{w}$ and $\bar{g}$, and standard deviation σ_w and σ_g, respectively. The exponential decay term describes the distance-dependent interaction to the vehicle in the front, and R characterized the interaction length. It is clear that, at higher vehicle densities, the acceleration due to the relative velocity is more pronounced since $w_n\Delta x_n/R$ is relatively smaller. Finally, λ represents the relative strength of the influence of the second term to the first term.

We employ the same disturbance propagation analysis to calculate the neutral stability boundary of this system. In the thermodynamic limit, and to the lowest order expansion of $(\sigma_w/\tilde{w}_0)^2$ and $(\sigma_g/\tilde{g}_0)^2$, the onset of the instability occurs when

$$f_1 > \frac{1}{2\tau\tilde{w}_0}\left(1 + \frac{2\sigma_w^2}{\tilde{w}_0^2}\right) + \frac{\lambda\tilde{g}_0}{\tau\tilde{w}_0}\left(1 + \frac{2\sigma_w^2}{\tilde{w}_0^2} - \frac{2\mathrm{Cov}\,(w,g)}{\tilde{w}_0\tilde{g}_0}\right)e^{-w_n\Delta x_n^{(0)}/R}, \tag{3.28}$$

where $\mathrm{Cov}(w,g)$ is the covariance of w_n and g_n. In the limit $\lambda \to 0$, Eq. (3.28) simply rediscovers the instability criterion derived in Eq. (3.23). First, let us consider the case where w_n and g_n are independent from each other, which means individual's distance perception is uncorrelated to individual's awareness of the relative velocity, hence, $\mathrm{Cov}(w,g) = 0$. The neutral stability boundary as a function of

$(\sigma_w/\tilde{w}_0)^2$ is shown Fig. 3.6. At high vehicle densities, the individual difference further inhibits the jamming transition as the relative velocity dependent acceleration rule is considered. The unjammed phase space opens up while the jammed phase space is further suppressed as the variation of distance perception increases, see the comparison of Fig. 3.1 and Fig. 3.6. It is quite intuitive since, if the distance to the vehicle in the front is close, the relative velocity dependent acceleration would slow down the vehicle as the vehicle in the front is slower. This mechanism helps to maintain distance between vehicles effectively, therefore, it suppresses the jamming transition. In addition, let us consider the other case where w_n equals to g_n, which means the driver who accelerates abruptly due to the change of the relative distance would also accelerate abruptly due to the change of relative velocity, hence, $\mathrm{Cov}(w, g) = \sigma_g^2 = \sigma_w^2$. Similar trend of the neutral stability boundary is observed, see Fig. 3.6. However, the correlation between w_n and g_n shrinks the unjammed phase space a little bit, since more abrupt change in the desired velocity makes the system easier to be jammed. On the contrary, it is expected that an anti-correlated w_n and g_n would help to inhibit traffic jam.

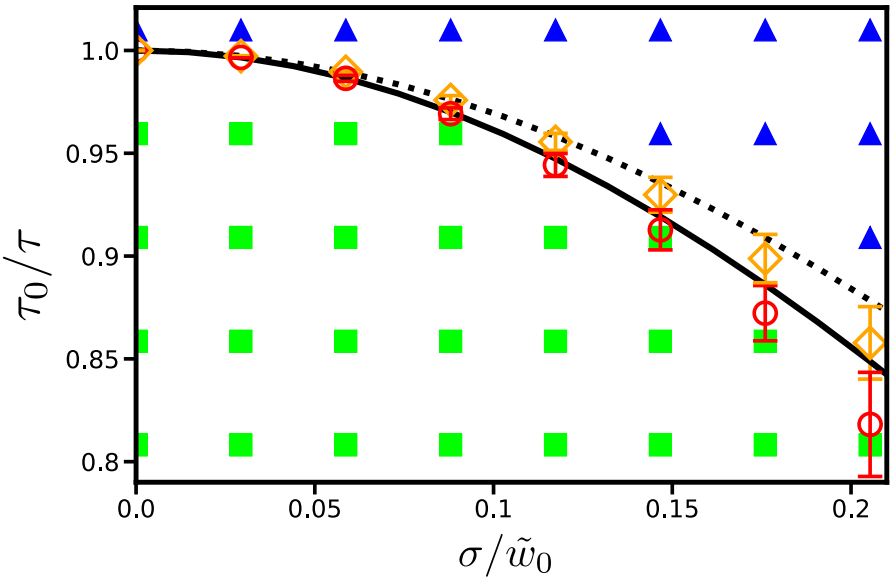

Figure 3.6: Phase diagram of the traffic system shown in Eq. (3.26). The black line plots the neutral stability boundary of Eq. (3.28) for $\mathrm{Cov}(w, g) = 0$, and solid green squares and solid blue triangles represent the jammed and unjammed state, respectively. Numerical simulations of Eq. (3.26) for $\mathrm{Cov}(w, g) = 0$ are shown in red circles. Orange diamonds and dotted line represent the result of simulations and analytical results, respectively, for the scenario where $w_n = g_n$. 100 realizations of Gaussian random fields are carried out for each simulation data point. The phase diagram is obtained for $R = 1$, $\lambda = 1$, $N/L = 1$, $h = 2$, and $N = 256$.

Chapter 4

Phenomenon and Simulation Results

The advantages of microscopic models are that they provide a way to understand the mechanics behind phenomenon in traffic systems. One of them is the "phantom traffic jam", which we have introduced in the introduction. In Bando's model, this phenomena can be explained as the competition between drivers' reaction times and intensity of changing drives' desired velocity due to varying the interval in front. Nonetheless, there are still many intriguing problems in traffic systems that remain unclear. In this chapter, phenomenon that can be partially reproduced by the Bando's and our model will be illustrated.

4.1 Hysteresis-like Phase Diagram

In chapter 2, we have shown the spontaneous phase separation when the traffic system transits from free flow into a jamming state. Since the system in Bando's model is closed, some local clusters of jamming state enclosed by free flow must be formed due to the number conservation. Therefore, most vehicles in a traffic system are either in clusters or in free flow. In 1994, Bando *et al.* observed that in the $\Delta x - v$ phase space, all vehicles in a traffic system will undergo a hysteresis-like close loop with two universal endpoints, $A = (\Delta x_C, v_C)$ and $B = (\Delta x_F, v_F)$, which are uncorrelated with the configuration of the system [21]. See Fig 4.1. It is interesting to note that the system is mainly composed of free flow

states and jamming states, with only a few vehicles on the interface between two states. Therefore, we can make use of this property with number conservation to approximate the backward velocity v_{back} of clusters. That is

$$\frac{v_F}{\Delta x_F} - \frac{v_C}{\Delta x_C} = \left(\frac{1}{\Delta x_F} - \frac{1}{\Delta x_C}\right) v_{back}. \tag{4.1}$$

Thus, the backward velocity is

$$v_{back} = \frac{\Delta x_C v_F - \Delta x_F v_C}{\Delta x_F - \Delta x_C}. \tag{4.2}$$

See Figure 4.2.

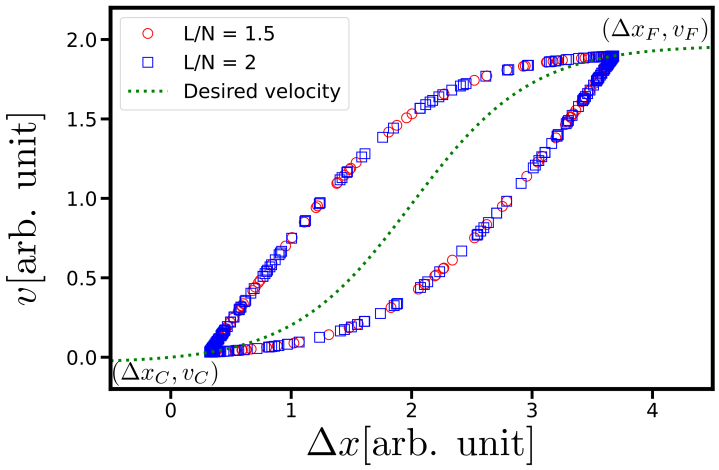

Figure 4.1: Hysteresis-like loops in the phase space of two systems with same vehicle numbers but different track lengths. The hysteresis loops formed by these two systems have the same size, which shows the irrelevance of hysteresis loops on the system size. Two simulations are done under configuration $N = 512$, $\tau = 1$, and h in the optimal velocity function is set at 2.

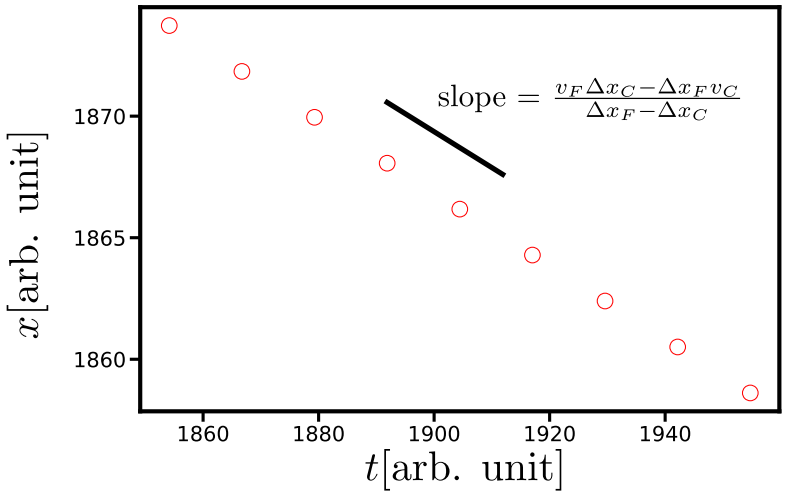

Figure 4.2: Propagation of wave front of the cluster. Simulations results show perfect predictions of analytical solutions. The simulation results are obtained for $N = 512$, $L/N = 1.5$, $\tau = 1$, and drivers are identical.

However, the empirical data shown in Fig 4.3 from Ref [1] reveals that the hysteresis loops in real traffic are not a single loop but widely scattered in the $\Delta x - v$ phase diagram. One possible way to regenerate this widely scattered hysteresis loops is taking individual differences into account. See Fig 4.4.

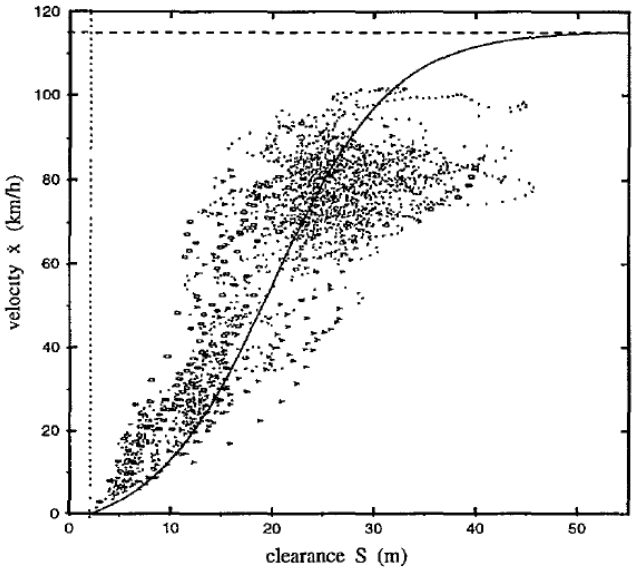

Figure 4.3: Empirical data in clearance-velocity phase space in Ref [1] Wide scattered data shows insufficiency of Bando's model. The parameters S and $\dot{x}$ in figure correspond to Δx and v, respectively, in our notation.

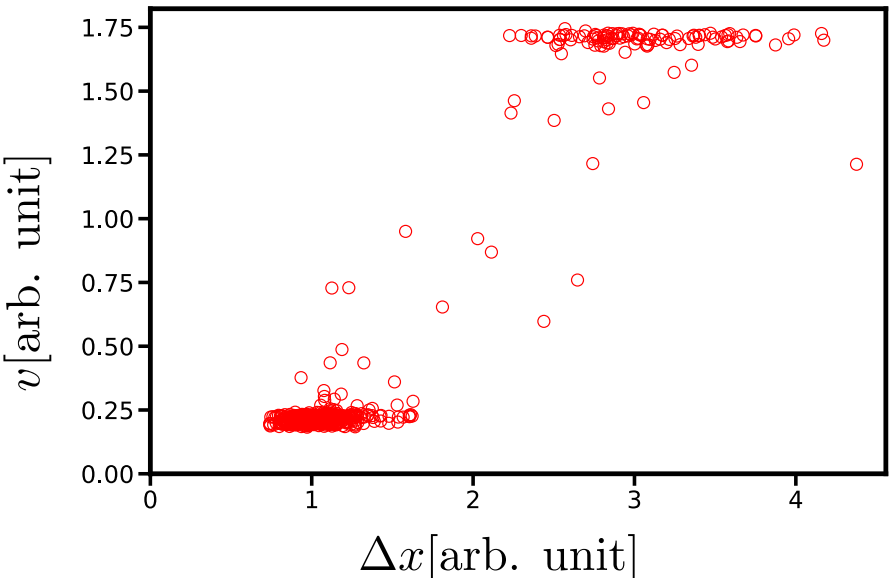

Figure 4.4: Widely scattered hysteresis loop obtained for individual difference $\sigma = 0.15$, $N = 512$, $L/N = 1.5$, and the relaxation time is set 0.05 beneath the threshold of neutral stability condition. Since there is no stationary state for a system with an individual difference, the shape of the hysteresis-like loop will vary with time, but widely scattered property accompany by individual differences is universal.

4.2 Scattering Fundamental Diagram

Another most intriguing but unclear phenomena is the scattering of density-flow fundamental diagram in the high-density region. See Fig 4.5 from Ref [2]. The wide scattering data means there is no definite relationship between traffic density and traffic flow. In recent years, scientists tried to analyze the mechanics behind this phenomena from different perspectives, such as interaction due to the lane changing process. In 1999, Treiber *et al.* simulated the macroscopic, gas-kinetic-based model, with considerations of different kinds of vehicles, such as trucks and cars in their researches. It was found that the fundamental diagram coming from the simulation with the existence of individual differences is similar to the empirical data. See Fig 4 in Ref [28]. In addition, a recent study by Tang *et al.* show the possible relationship between individual difference and the scattered data.

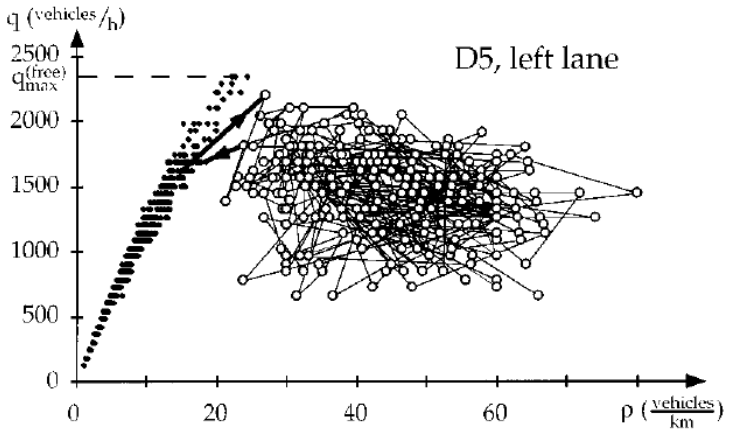

Figure 4.5: Empirical wide scattered fundamental diagram obtained by B. S. Kerner *et al.* in Ref [2]. Wide scattered data in the figure shows unclear correlations between traffic density ρ and traffic flow q.

The widely scattered data in Fig 4.4 also implies the possible relationship between individual differences and widely scattered fundamental diagram. Simulation results are shown in Fig 4.6. Since the mean-field concept of density prohibits the dramatic changing of physical parameters in a unit volume element, the simulation data exclude drivers who locate at the phase boundary. Therefore, traffic density is defined as the inverse of the average value of intervals between drivers

and the nearest vehicles in front only in jamming or free flow states, and traffic flow is obtained by multiply the density and the corresponding average velocity.

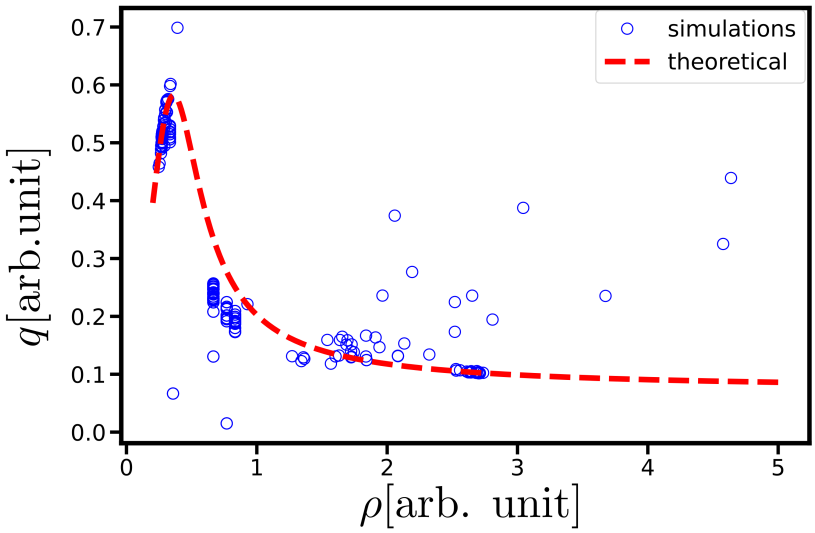

Figure 4.6: Simulation fundamental diagram obtained for $N = 512$, $\tau = 1$, $\sigma = 0.3$, and multiple different global densities $N/L = 1/1.2$, $1/1.3$, $1/1.4$, $1/1.5$, $1/2.8$, $1/2.9$, $1/3$. Numerical results show a possible relationship between wide scattered fundamental diagram and individual difference.

In this chapter, phenomenon with wide scattered properties in the $\Delta x - v$ phase space and the fundamental diagram are introduced. Simulation results show the potential relationship between widely scattered data and the individual difference. Nonetheless, the mechanisms behind these phenomenon are still unclear since they can only be observed after the system has experienced jamming transition, which means analytical analysis must be extended to nonlinear regions and analytical solutions are always difficult to be deduced. Even though the difficulties in obtaining analytical solutions in nonlinear regions, Nagatani *et al.* presented a possible method to approach analytical solutions in weak nonlinear regions [36]. Therefore, it is our interest to understand the influence of individual differences in weak nonlinear regions in our future works. Other possible future works will be organized in the next chapter.

Chapter 5

Summary and Discussion

We investigate how the individual difference of drivers affects the jamming instability by implementing different distance perceptions using Gaussian random fields in Bando's optimal velocity model. Both simulation results and perturbation calculations show that, at high vehicle densities, the onset of the jamming instability is effectively suppressed if individual differences are introduced. Contradictorily, the instability is augmented at low vehicle densities. To further understand the physical mechanism of jamming instability, we analyze how the spatial disturbance in the relative distance propagates through the traffic. We find that drivers with good distance perception reduce the disturbance while drivers with poor distance perception amplify it. Therefore, we show that whether the instability occurs depends on the overall distribution of the distance perception rather than the details of the spatial ordering of vehicles. This indicates that the individual difference of drivers would also suppress the traffic jam for traffic systems that allow vehicles to pass by one another.

The universality of individual difference induced jamming suppression can be further elucidated by considering a more general form of the desired velocity. We get

$$\ddot{x}_n = \frac{V(w_n \Delta x_n, g_n \Delta v_n) - \dot{x}_n}{\tau}, \tag{5.1}$$

where $V(w_n \Delta x_n, g_n \Delta v_n)$ is the generalized desired velocity which monotonically increases as the distance to the vehicle in the front increases or as the relative velocity increases. Employing the disturbance propagation analysis, we find that

the onset of the instability occurs when

$$V_x > \frac{1}{\tilde{w}_0 \tau}\left[\left(1+\frac{2\sigma^2}{\tilde{w}_0^2}\right)\left(\frac{1}{2}+V_v\tilde{g}_0\right)-\frac{2V_v \mathrm{Cov}(w,g)}{\tilde{w}_0}\right], \tag{5.2}$$

where $V_x = (\partial V/\partial \Delta x_n)/w_n$ and $V_v = (\partial V/\partial \Delta v_n)/g_n$, both evaluated at $\Delta x_n = \Delta x_n^{(0)}$ and $\Delta v_n = 0$. It is clear that the jamming instability is influenced by individual differences in several different aspects. First, the slight decrease in the steady state velocity due to the variation of individual distance perception gives rise to a relatively slow change in the desired velocity as the distance changes at high vehicle densities and vice versa, which inhibits and promotes the jamming transition at high and low vehicle densities, respectively. This conclusion is universal since the desired velocity function has to saturate to certain values at both ends of the vehicle density, which warrants an inflection point (density) for the desired velocity function. Therefore, the rate of the change in the desired velocity due to variation of distance perception would be either smaller or larger depending on the vehicle density. Past work has shown that the inflection point is crucial in analyzing nonlinear wave in the jammed state [15, 36, 37, 38, 39]. Second, the term $V_v\tilde{g}_0$ always inhibits the jamming transition since the relative velocity dependent acceleration would effectively help to maintain proper distance between vehicles. Furthermore, the correlation between the distance perception and relative velocity awareness of drivers is shown to affect the jamming transition as well, since the correlation could further enhance the abruptness of the velocity change.

In this study, we show that the individual difference has a pronounced effect on the onset of the jamming instability. However, mechanisms for influencing jamming transition in real traffic due to heterogeneity remain unclear. For example, it has been observed that one heterogeneity in traffic system is the log-normal distribution of perception-reaction time, which might be interpreted as drivers' reaction time [40, 41]. The analytical process should be slightly modified since the random field property in Fourier space might be different between Gaussian and log-normal distribution. Also, Bando's model has been criticized for being poor at reproducing real traffic, such as synchronized flow in empirical three phases model [33]. This is because there are plenty of artificial, unreal assumptions used in the optimal velocity model, such as closed systems. It has been shown that there exists a richer phase diagram in an open system [34]. In 2003, Trieber *et al.* introduced

a simple "memory effect" into the one-dimensional intelligent driver model, and presented a possible way to regenerate synchronized flow in open traffic systems without taking drivers' individual difference, lane changing behaviors, and ramps into account [42]. Nevertheless, Bando's model still provides a probable way to approach the real traffic, and similar results might be possible by introducing these effects into the optimal velocity model.

Therefore, it is of interest to extend the current model to explore how the individual difference affects the traffic flow, in particular, of the jammed state under more realistic conditions. That is to see the effect of individual differences on the relation between the traffic flow and the vehicle density (i.e., the fundamental diagram). Since we have shown that the variation of distance perception leads to changes in the steady-state velocity, the individual difference could be responsible for the wide scattering nature of the fundamental diagram. Furthermore, investigation of the influences of heterogeneity due to individual difference can be extended to nonlinear regions.

In conclusion, this work discusses how individual differences influence the onset of jamming transition when the traffic system is set as a single lane in a closed-loop, and passing is prohibited. Jamming suppression in high density is observed when individual differences exist, and the onset of jamming transition is irrelevant of drivers' spatial order. But there are still other interesting prospects that we can investigate in our future works. For example, the influence of heterogeneity when taking other realistic factors into account. Different behaviors in nonlinear regions between identical drivers and drivers with individual differences is also an intriguing topic.

Appendix

A. Calculation of second perturbation

According to the equation (3.14), the zeroth order perturbation of m^{th} Fourier mode is

$$\lambda_m^{(0)} = \tilde{w}_0 \left(e^{i\alpha_m} - 1 \right). \tag{3}$$

Since the ensemble average of non-zero Fourier mode amplitude of Gaussian random field is σ^2/N. The second order perturbation can be rewritten as

$$\begin{aligned}
\lambda_m^{(2)} &= \sum_{k \neq m} \frac{|\tilde{w}_{m-k}|^2 \left(e^{i\alpha_m} - 1\right)\left(e^{i\alpha_k} - 1\right)}{\tilde{w}_0 \left(e^{i\alpha_m} - e^{i\alpha_k}\right)} \\
&\simeq \frac{\sigma^2}{N\tilde{w}_0} \sum_{k \neq m} \frac{\left(e^{i\alpha_m} - 1\right)\left(e^{i\alpha_k} - 1\right)}{\left(e^{i\alpha_m} - e^{i\alpha_k}\right)} \\
&= \frac{\sigma^2}{N\tilde{w}_0} \sum_{k \neq m} \frac{\left(e^{i\alpha_m} - 1\right)\left(e^{i\alpha_k} - 1\right)\left(e^{-i\alpha_m} - e^{-i\alpha_k}\right)}{\left(e^{i\alpha_m} - e^{i\alpha_k}\right)\left(e^{-i\alpha_m} - e^{-i\alpha_k}\right)} \\
&= \frac{\sigma^2}{N\tilde{w}_0} \sum_{k \neq m} \frac{\left(e^{i\alpha_{m+k}} - e^{i\alpha_k} - e^{i\alpha_m} + 1\right)\left(e^{-i\alpha_m} - e^{-i\alpha_k}\right)}{2 - e^{i\alpha_{k-m}} - e^{i\alpha_{m-k}}} \\
&= \frac{\sigma^2}{N\tilde{w}_0} \sum_{k \neq m} \frac{e^{i\alpha_k} - e^{i\alpha_{k-m}} - 1 + e^{-i\alpha_m} - e^{i\alpha_m} + 1 + e^{i\alpha_{m-k}} - e^{-i\alpha_k}}{2 - 2\cos\alpha_{k-m}}
\end{aligned} \tag{4}$$

Let $n = k - m$, we can deduce

$$\begin{aligned}
\lambda_m^{(2)} &= \frac{\sigma^2}{N\tilde{w}_0} \sum_{n \neq 0} \frac{e^{i\alpha_{n+m}} - e^{-i\alpha_{n+m}} - e^{i\alpha_n} + e^{-i\alpha_n} + e^{-i\alpha_m} - e^{i\alpha_m}}{2 - 2\cos\alpha_n} \\
&= \frac{i\sigma^2}{N\tilde{w}_0} \sum_{n \neq 0} \frac{\sin\alpha_n \cos\alpha_m + \cos\alpha_n \sin\alpha_m - \sin\alpha_n - \sin\alpha_m}{1 - \cos\alpha_n} \\
&= \frac{i\sigma^2}{N\tilde{w}_0} \sum_{n \neq 0} \frac{\left(\sin\alpha_n \cos\alpha_m + \cos\alpha_n \sin\alpha_m - \sin\alpha_n - \sin\alpha_m\right)\left(1 + \cos\alpha_n\right)}{\sin^2\alpha_n}.
\end{aligned} \tag{5}$$

Since

$$\begin{aligned}
&(\sin\alpha_n\cos\alpha_m+\cos\alpha_n\sin\alpha_m-\sin\alpha_n-\sin\alpha_m)(1+\cos\alpha_n)\\
=&\sin\alpha_n\cos\alpha_m+\cos\alpha_n\sin\alpha_m-\sin\alpha_n-\sin\alpha_m\\
&+\cos\alpha_n\sin\alpha_n\cos\alpha_m+\cos^2\alpha_n\sin\alpha_m-\cos\alpha_n\sin\alpha_n-\cos\alpha_n\sin\alpha_m\\
=&\sin\alpha_n\cos\alpha_m-\sin\alpha_n+\cos\alpha_n\sin\alpha_n\cos\alpha_m-\sin^2\alpha_n\sin\alpha_m-\cos\alpha_n\sin\alpha_n.
\end{aligned}$$

Therefore

$$\begin{aligned}
\lambda_m^{(2)}&=\frac{i\sigma^2}{N\tilde{w}_0}\left(-N\sin\alpha_m+\sum_{n\neq 0}\frac{\sin\alpha_n\cos\alpha_m-\sin\alpha_n+\cos\alpha_n\sin\alpha_n\cos\alpha_m-\cos\alpha_n\sin\alpha_n}{\sin^2\alpha_n}\right)\\
&=\frac{i\sigma^2}{N\tilde{w}_0}\left(-N\sin\alpha_m+\sum_{n\neq 0}\frac{\cos\alpha_m-1+\cos\alpha_n\cos\alpha_m-\cos\alpha_n}{\sin\alpha_n}\right).
\end{aligned}\tag{6}$$

The second identity is zero because no matter what the number of vehicles N is, we can always find the counterpart in equation(6) such that the summation would be vanished. For example we can find

$$\frac{1}{\sin\alpha_j}+\frac{1}{\sin\alpha_{-j}}=0.\tag{7}$$

Since the summation doesn't include the zero-th mode. The only term we can't find the counterpart to eliminate is when the number of vehicles N is even number and $k=-N/2$, which means $\alpha_n=-\pi$. However, since

$$\lim_{\alpha_n\to-\pi}\frac{\cos\alpha_m-1+\cos\alpha_n\cos\alpha_m-\cos\alpha_n}{\sin\alpha_n}=0.\tag{8}$$

we can reduce the second perturbation to

$$\lambda_m^{(2)}=-\frac{i\sigma^2}{\tilde{w}_0}\sin\alpha_m.\tag{9}$$

The equation of motion about k^{th} Fourier mode up to second perturbation can be write as

$$\ddot{\tilde{y}}_k+\frac{1}{\tau}\dot{\tilde{y}}_k=\frac{f}{\tau}\tilde{w}_0\left(\cos\alpha_k-1+i\left(1-\frac{\sigma^2}{\tilde{w}_0^2}\right)\sin\alpha_k\right)\tag{10}$$

The phase boundary can be found by assuming the periodic motion of Fourier mode $\tilde{y}_k\propto e^{ivt},\ v\in\mathbb{R}$. Thus

$$\begin{cases}
v=f\tilde{w}_0\left(1-\frac{\sigma^2}{\tilde{w}_0^2}\right)\sin\alpha_k\\
-v^2=\frac{f}{\tau}\tilde{w}_0\left(\cos\alpha_k-1\right)
\end{cases}\tag{11}$$

Combining these two equations, we can get the boundary condition will be

$$f = \frac{1}{2\tau\tilde{w}_0 \left(1 - \sigma^2/\tilde{w}_0^2\right)^2 \cos^2(\alpha_k/2)} \tag{12}$$

B. Calculation of propagation distribution

The equation (3.22) shows the stability of traffic system can be determined by multiplication

$$z \equiv \prod_n \frac{fw_n}{\sqrt{(fw_n - \Omega^2\tau)^2 + \Omega^2}}.$$

Thus

$$\begin{aligned}
\frac{1}{z^2} &= \prod_n \frac{(fw_n - \Omega^2\tau)^2 + \Omega^2}{f^2 w_n^2} \\
&= \prod_n \frac{f^2 w_n^2 - 2fw_n\Omega^2\tau + \Omega^4\tau^2 + \Omega^2}{f^2 w_n^2} \\
&\simeq \prod_n \left(1 - \frac{2\Omega^2\tau}{fw_n} + \frac{\Omega^2}{f^2 w_n^2}\right) \\
&\simeq 1 + \sum_n \left(-\frac{2\Omega^2\tau}{fw_n} + \frac{\Omega^2}{f^2 w_n^2}\right).
\end{aligned} \tag{13}$$

Since

$$\begin{aligned}
\sum_n \frac{1}{w_n} &= \sum_n \frac{1}{\tilde{w}_0\left(1 + \Delta_n/\tilde{w}_0\right)} \\
&\simeq \frac{1}{\tilde{w}_0} \sum_n \left(1 - \frac{\Delta_n}{\tilde{w}_0} + \frac{\Delta_n^2}{\tilde{w}_0^2}\right) \\
&= \frac{N}{\tilde{w}_0}\left(1 + \frac{\sigma^2}{\tilde{w}_0^2}\right),
\end{aligned}$$

and

$$\begin{aligned}
\sum_n \frac{1}{w_n^2} &= \sum_n \frac{1}{\tilde{w}_0^2\left(1 + \Delta_n/\tilde{w}_0\right)^2} \\
&= \sum_n \frac{1}{\tilde{w}_0^2\left(1 + 2\Delta_n/\tilde{w}_0 + \Delta_n^2/\tilde{w}_0^2\right)^2} \\
&\simeq \frac{1}{\tilde{w}_0} \sum_n \left(1 - \frac{\Delta_n}{\tilde{w}_0} - \frac{\Delta_n^2}{\tilde{w}_0^2} + 4\frac{\Delta_n^2}{\tilde{w}_0^2}\right) \\
&\simeq \frac{1}{\tilde{w}_0} \sum_n \left(1 - \frac{\Delta_n}{\tilde{w}_0} + 3\frac{\Delta_n^2}{\tilde{w}_0^2}\right) \\
&= \frac{N}{\tilde{w}_0}\left(1 + 3\frac{\sigma^2}{\tilde{w}_0^2}\right).
\end{aligned}$$

We can deduce the multiplication up to the second order of individual difference σ

$$\frac{1}{z^2} = 1 + \left(-\frac{2\tau}{f}\frac{N}{\tilde{w}_0}\left(1 + \frac{\sigma^2}{\tilde{w}_0}\right) + \frac{1}{f^2}\frac{N}{\tilde{w}^2}\left(1 + 3\frac{\sigma^2}{\tilde{w}_0^2}\right)\right) + \mathcal{O}\left(\sigma^4\right) \tag{14}$$

Then

$$z = \frac{1}{\sqrt{1 + \left(-\frac{2\tau}{f}\frac{N}{\tilde{w}_0}\left(1 + \frac{\sigma^2}{\tilde{w}_0}\right) + \frac{1}{f^2}\frac{N}{\tilde{w}^2}\left(1 + 3\frac{\sigma^2}{\tilde{w}_0^2}\right)\right)}} \tag{15}$$

$$\simeq 1 - \frac{1}{2}\left[-\frac{2\tau}{f}\frac{N}{\tilde{w}_0}\left(1 + \frac{\sigma^2}{\tilde{w}_0}\right) + \frac{1}{f^2}\frac{N}{\tilde{w}^2}\left(1 + 3\frac{\sigma^2}{\tilde{w}_0^2}\right)\right] \tag{16}$$

$$= 1 - \frac{N}{2(f\tilde{w}_0)^2}\left[\left(1 + 3\frac{\sigma^2}{\tilde{w}_0^2}\right) - 2\tau f\tilde{w}_0\left(1 + \frac{\sigma^2}{\tilde{w}_0}\right)\right] + \mathcal{O}\left(\sigma^4\right) \tag{17}$$

Bibliography

[1] Masako Bando, Katsuya Hasebe, Ken Nakanishi, Akihiro Nakayama, Akihiro Shibata, and Yuki Sugiyama. Phenomenological study of dynamical model of traffic flow. *J. Phys. I France*, 5(11):1389–1399, 1995.

[2] B. S. Kerner and H. Rehborn. Experimental properties of complexity in traffic flow. *Phys. Rev. E*, 53:R4275–R4278, May 1996.

[3] Michael E. Cates and Julien Tailleur. Motility-induced phase separation. *Annual Review of Condensed Matter Physics*, 6(1):219–244, 2015.

[4] M. C. Marchetti, J. F. Joanny, S. Ramaswamy, T. B. Liverpool, J. Prost, Madan Rao, and R. Aditi Simha. Hydrodynamics of soft active matter. *Rev. Mod. Phys.*, 85:1143–1189, Jul 2013.

[5] B.d. Greenshields, J.r. Bibbins, W.s. Channing, and H.h. Miller. A study of traffic capacity. *Highway Research Board proceedings*, 1935:–, 1935.

[6] Dirk Helbing. Traffic and related self-driven many-particle systems. *Rev. Mod. Phys.*, 73:1067–1141, Dec 2001.

[7] Louis A. Pipes. An operational analysis of traffic dynamics. *Journal of Applied Physics*, 24(3):274–281, 1953.

[8] Robert E. Chandler, Robert Herman, and Elliott W. Montroll. Traffic dynamics: Studies in car following. *Operations Research*, 6(2):165–184, 1958.

[9] Denos C. Gazis, Robert Herman, and Richard W. Rothery. Nonlinear follow-the-leader models of traffic flow. *Operations Research*, 9(4):545–567, 1961.

[10] G. F. Newell. Nonlinear effects in the dynamics of car following. *Operations Research*, 9(2):209–229, 1961.

[11] M. Bando, K. Hasebe, A. Nakayama, A. Shibata, and Y. Sugiyama. Dynamical model of traffic congestion and numerical simulation. *Phys. Rev. E*, 51:1035–1042, Feb 1995.

[12] Kai Nagel and Michael Schreckenberg. A cellular automaton model for freeway traffic. *J. Phys. I France*, 2(12):2221–2229, 1992.

[13] Kai Nagel and Hans J. Herrmann. Deterministic models for traffic jams. *Physica A: Statistical Mechanics and its Applications*, 199(2):254 – 269, 1993.

[14] Dirk Helbing and Benno Tilch. Generalized force model of traffic dynamics. *Phys. Rev. E*, 58:133–138, Jul 1998.

[15] Takashi Nagatani. The physics of traffic jams. *Reports on Progress in Physics*, 65(9):1331–1386, aug 2002.

[16] Michael James Lighthill and Gerald Beresford Whitham. On kinematic waves ii. a theory of traffic flow on long crowded roads. *Proceedings of the Royal Society of London. Series A. Mathematical and Physical Sciences*, 229(1178):317–345, 1955.

[17] Paul I. Richards. Shock waves on the highway. *Operations Research*, 4(1):42–51, 1956.

[18] G. B. Whitham. *Linear and Nonlinear Waves*. John Wiley, 1974.

[19] I. Prigogine and F. C. Andrews. A boltzmann-like approach for traffic flow. *Operations Research*, 8(6):789–797, 1960.

[20] S.L. Paveri-Fontana. On boltzmann-like treatments for traffic flow: A critical review of the basic model and an alternative proposal for dilute traffic analysis. *Transportation Research*, 9(4):225 – 235, 1975.

[21] M. Bando, K. Hasebe, A. Nakayama, A. Shibata, and Y. Sugiyama. Structure stability of congestion in traffic dynamics. *Japan Journal of Industrial and Applied Mathematics*, 11(2):203, 1994.

[22] Yu-barki Sugiyama and Hiroyasu Yamada. Simple and exactly solvable model for queue dynamics. *Phys. Rev. E*, 55:7749–7752, Jun 1997.

[23] B. S. Kerner and H. Rehborn. Experimental properties of phase transitions in traffic flow. *Phys. Rev. Lett.*, 79:4030–4033, Nov 1997.

[24] M. Rickert, K. Nagel, M. Schreckenberg, and A. Latour. Two lane traffic simulations using cellular automata. *Physica A: Statistical Mechanics and its Applications*, 231(4):534 – 550, 1996.

[25] Peter Wagner, Kai Nagel, and Dietrich E. Wolf. Realistic multi-lane traffic rules for cellular automata. *Physica A: Statistical Mechanics and its Applications*, 234(3):687 – 698, 1997.

[26] Anthony D. Mason and Andrew W. Woods. Car-following model of multi-species systems of road traffic. *Phys. Rev. E*, 55:2203–2214, Mar 1997.

[27] B. Tilch and D. Helbing. Evaluation of single vehicle data in dependence of the vehicle-type, lane, and site. In Dirk Helbing, Hans J. Herrmann, Michael Schreckenberg, and Dietrich E. Wolf, editors, *Traffic and Granular Flow '99*, pages 333–338, Berlin, Heidelberg, 2000. Springer Berlin Heidelberg.

[28] Martin Treiber and Dirk Helbing. Macroscopic simulation of widely scattered synchronized traffic states. *Journal of Physics A: Mathematical and General*, 32(1):L17–L23, jan 1999.

[29] Geng Zhang, Di-Hua Sun, Hui Liu, and Min Zhao. Analysis of drivers' characteristics in car-following theory. *Modern Physics Letters B*, 28(24):1450191, 2014.

[30] David Herrero-Fernández. Psychophysiological, subjective and behavioral differences between high and low anger drivers in a simulation task. *Transportation Research Part F: Traffic Psychology and Behaviour*, 42:365 – 375, 2016. Advances in Driving Anger.

[31] Tieqiao Tang, Chuanyao Li, Haijun Huang, and Huayan Shang. A new fundamental diagram theory with the individual difference of the driver's perception ability. *Nonlinear Dynamics*, 67(3):2255–2265, Feb 2012.

[32] Jun-Fang Tian, Bin Jia, and Xing-Gang Li. A new car following model: Comprehensive optimal velocity model. *Communications in Theoretical Physics*, 55(6):1119–1126, jun 2011.

[33] Boris S. Kerner. *The Physics of Traffic*. Springer-Verlag Berlin Heidelberg, 2004.

[34] G. Schütz and E. Domany. Phase transitions in an exactly soluble one-dimensional exclusion process. *Journal of Statistical Physics*, 72(1):277–296, 1993.

[35] Masuyuki Hitsuda Takeyuki Hida. *Gaussian Processes*. American Mathematical Society, 1993.

[36] Takashi Nagatani. Density waves in traffic flow. *Phys. Rev. E*, 61:3564–3570, Apr 2000.

[37] Teruhisa S. Komatsu and Shin-ichi Sasa. Kink soliton characterizing traffic congestion. *Phys. Rev. E*, 52:5574–5582, Nov 1995.

[38] Takashi Nagatani. Thermodynamic theory for the jamming transition in traffic flow. *Phys. Rev. E*, 58:4271–4276, Oct 1998.

[39] Masakuni Muramatsu and Takashi Nagatani. Soliton and kink jams in traffic flow with open boundaries. *Phys. Rev. E*, 60:180–187, Jul 1999.

[40] Nathan Gartner, C. Messer, and A. Rathi. *Traffic Flow Theory: A State-of-the-Art Report*. 01 2001.

[41] Ludovic Leclercq, Lei Zhang, Shengrui Zhang, Bei Zhou, Shuaiyang Jiao, and Yan Huang. An improved car-following model considering desired safety distance and heterogeneity of driver's sensitivity. *Journal of Advanced Transportation*, 2021:6693433, 2021.

[42] Martin Treiber and Dirk Helbing. Memory effects in microscopic traffic models and wide scattering in flow-density data. *Phys. Rev. E*, 68:046119, Oct 2003.